POLITECNICO DI TORINO
Repository ISTITUZIONALE

Liquid-state pyroelectric energy harvesting

Original
Liquid-state pyroelectric energy harvesting / Bevione, M., Garofalo, E., Cecchini, L., Chiolerio, A.. - In: MRS ENERGY & SUSTAINABILITY. - ISSN 2329-2229. - ELETTRONICO. - 7:E38(2020). [10.1557/mre.2020.39]

Availability:
This version is available at: 11583/2853668 since: 2021-06-07T12:37:03Z

Publisher:
Material Research Society, Cambridge University Press

Published
DOI:10.1557/mre.2020.39

Terms of use:

This article is made available under terms and conditions as specified in the corresponding bibliographic description in the repository

Publisher copyright
Nature --> vedi Generico

[DA NON USARE] ex default_article_draft

(Article begins on next page)

19 November 2026

Liquid state pyroelectric energy harvesting

M. Bevione [1], E. Garofalo [1,2], L. Cecchini [1,2] and A. Chiolerio [1,*]

[1] Istituto Italiano di Tecnologia, Center for Sustainable Future Technologies, Via Livorno 60, 10144 Torino, Italy;

[2] Politecnico di Torino, Department of Electronics, Corso Duca degli Abruzzi 24, 10129 Torino, Italy;

***** Correspondence: alessandro.chiolerio@iit.it; Tel.: +39 011 5091903

Received: date; Accepted: date; Published: date

Summary: A liquid state pyroelectric energy harvester is described, providing a remarkable capacity to convert a thermal gradient into electrical energy

Abstract: Increasing the sustainability of energy generation can be pursued by harvesting extremely low enthalpy sources: low temperature differences between cold and hot reservoirs are easily achieved in every industrial process, both at large and at small scale, in plants as well as in small appliances, vehicles, natural environments, human bodies. This paper presents the assessment and efficiency estimate of a liquid state pyroelectric energy harvester, based on a colloid containing barium titanate nanoparticles and ferrofluid as stabilizer. The liquid is set in motion by an external pump to control velocity, in a range similar to the one achieved by Rayleigh - Bénard convection, and the colloid reservoir is heated. The colloid is injected into a Fluorinated Ethylene Propylene pipe where titanium electrodes are placed to collect electrical charges generated by pyroelectricity on the surface of the nanoparticles. reaching 22.4 % of the ideal Carnot efficiency of a thermal machine working on the same temperature drop. The maximum extracted electrical power per unit of volume is above 7 mW/m^3 with a ΔT between electrodes of 3.9 K.

Discussion points:

- For the first time, a liquid pyroelectric generator featuring galvanic extraction was demonstrated
- Any triboelectric contribution was separated from the pyroelectric one to estimate conversion efficiency
- A comprehensive theoretical framework is proposed, to interpret data
- Charge transfer phenomena occurring at liquid / solid interfaces lack understanding

Keywords: pyroelectric effect; energy harvesting; colloid; liquid energy harvester; waste heat to power.

1. Introduction

In recent years, the impact of economic growth on energy consumption has become increasingly important. Its implications on the emission of polluting agents are now well known as well as the obvious consequences on climatic conditions. According to the last International Energy Outlook (IEO) of the U.S. Energy Information Administration (EIA), the world energy consumption is expected to grow by approximately 15 % for the countries members of Organization of Economic Cooperation and Development (OECD) and by approximately 70 % for the others, in the years ranging from 2018 to 2050 [1]. Analysing the data provided by the 68th edition of the BP Statistical Review of World Energy [2], it is possible to provide an estimate of the global consumption forecast for 2050: according to them, OECD countries will contribute to the energy balance with a demand of $\approx 76 \cdot 10^3$ TWh/year, whereas non-OECD will require $\approx 162 \cdot 10^3$ TWh/year, almost exactly matching 2018 overall consumption ($\approx 161 \cdot 10^3$ TWh/year). Thermodynamic limits of energy conversion processes unavoidably lead to a concurrent waste heat generation and for this reason the research here described is focused on the development of harvesting systems to limit dispersions and increase efficiencies, which translates in a better exploitation of the energy available instead of a larger production.

Usually, energy is dumped into the environment in four forms: vibro-acoustic waves including dissipated heat, electromagnetic waves, chemical potential and in particular cases sub-nuclear particles. The former arises a strong interest for the process efficiency enhancement. According to the study conducted by Forman *et al.* [3], 72 % of the global primary energy consumption is lost after conversion under the form of heat that could be recovered. This field is called waste heat recovery (WHR), which groups all those techniques able to exploit heat at high temperatures to accumulate energy or to transform it again in a profitable potential, or waste heat to power (WHP), where heat is used to generate electrical power avoiding emission and combustion. In general, waste heat can be distinguished in three classes depending on its quality, namely high (HG), medium (MG) and low-grade (LG) having temperatures above 500°C, between 200 and 500°C and below 200°C respectively. In the same study [3], it is underlined that the largest part of wasted heat, about 63 % of the total, is introduced into the environment at a very low temperature (LG class). For this reason, the interest of research in the development of systems able to recover this particular low-quality form of energy is increasing.

LG waste heat is by far the most challenging class to be harvested because of its heat content. Even though the largest part of the emissions comes from industrial processes [1], responsible for more than 50 % of the overall energy consumption, devices for its recovery have been developed in several application fields using different approaches. The vapour compression systems, used in coolers, heat pumping or dehumidifiers, employs a coolant to capture heat and, e.g. by mean of evaporation, cool the air [4]. Adsorption cycles by means of a four-step thermodynamic cycle, i.e. pressurization, desorption, depressurization and adsorption, provide a cooling effect [5]. Among thermodynamic cycles,

Organic Rankine (ORC) and Kalina (KC) have shown to provide very good results in LG waste heat harvesting for power production. The former is based on the usage of hydrocarbon-based working fluids which, absorbing heat, evaporate passing through a turbine before condense newly [6]. Further details regarding current and new WHR/WHP technologies are provided in [7].

Another very popular harvesting method, particularly exploited in industrial and wearables fields, is based on the thermoelectric (TE) effect. Of great importance in this frame are the works of Vladimir Leonov *et al.* for the development of devices, like pulse oximeters [8], wearable thermopiles [9], EEG [10] or watches [11], completely supplied by body wasted heat. Whenever an temperature fluctuation in time appears, the pyroelectric (PyE) effect occurs and is exploited in PyE generators. Pyroelectricity is the ability of certain materials, having specific crystalline structures, of developing a spontaneous polarization once they have undergone a temporal temperature variation, and often appears with a piezoelectric (PE) response [7]. Several PyE nanogenerators have been proposed to convert thermal energy into electricity with attention on the wearable field [12]. An overview on the state of the art is provided in [13].

All devices developed in the works mentioned so far, with few exceptions, are solid-state devices, needing a large area of application to ensure good harvesting efficiency when dealing with LG sources. Moreover, their nature is not compliant with curved surfaces, or does not allow bending and stretching. Thus, the idea to combine solid and liquid properties to achieve better results in harvesting efficiency for applications where flexibility is fundamental, exploiting the properties of nano-materials, comes straightforward. The use of colloids, defined as solid nanoparticles dispersed in a carrier fluid, is our natural framework, in a study that starts from a toroidal dynamo (TORODYNA) exploiting thermomagnetic advection [14], encompasses triboelectric colloids [15] and finally aims at creating colloidal energy systems [16].

Here, an experimental apparatus for monitoring the short circuit current and open circuit voltage production brought by the PyE colloid under different heating conditions is presented. The colloid under analysis is a dispersion of barium titanate ($BaTiO_3$, BT) nanoparticles (NPs), having average diameter of 300 nm, dispersed in a ferrofluid (FF) suspension in kerosene solvent. FF, particularly stable from a gravitational point of view, was added to the composition with the aim of stabilizing BT and hindering precipitation. The functional colloid is heated up in a reservoir by means of a heating plate and then forced using a peristaltic pump into a fluorinated ethylene propylene (FEP) pipe [15]. Along the loop the fluid is subject to forced convection cooling. In order to collect the electrostatic charges developed thanks to the PyE and carried by the BT Nps, two titanium electrodes are placed along the pipe going in direct contact with the colloid. An external circuit is used to measure the open circuit voltage and the closed-circuit current.

The closest literature prior art is the work of Abdullahi Isse [17], where a hybridized pyro-piezo ferrofluidic wearable harvester exploiting body motion is proposed. It uses mainly the vibrations produced during walking or running, and

temperature variations are exploited to induce current by means of induction or pyro-piezo electric effects. The combination of all these currents resulted in 11.4 mA with a pyroelectric current of 3.03 nA. Another interesting work is the one of Lufan Jin *et al.* [18] where a colloidal wurtzite structure CdSe/ZnS quantum dots photodetector based on PyE is described. Here a layer of pyroelectric colloid is placed between two gold electrodes producing a current whenever the light at a specific wavelength hits the device.

2. Materials and Methods

Kerosene (purchased from Carlo Erba) was chosen as solvent because of its compatibility with the ferrofluid carrier fluid, was mixed with 2 % volume of FF (Ferrotech EFH3) to guarantee the dispersion of BT NPs (purchased from Inframat® Advanced Materials™) added in it in quantity equal to 0.5 %vol of the overall mixture (named KBT05, hereinafter). Barium Titanate NPs [19] have an average diameter of 300 nm and a tetragonal crystalline structure, which is needed to exhibit the PyE behaviour. The particles were dispersed by ultrasonication using a horn sonicator (Branson Digital Sonifier® Model 450) performed for 30 minutes at 100 W, with a duty cycle of 10 s of rest each 10 s of operation. To ensure homogeneous dispersion during the entire duration of the experiments, a magnetic stirrer (Velp Scientifica) was used. This is equipped with a heating plate used to provide different temperature conditions to the suspension.

The peristaltic pump (Ismatec MCP) is equipped with a rotor system coupled with silicone pipes having outer diameter (OD) of 4 mm and inner diameter (ID) of 3.2 mm. The central part of the apparatus is a FEP pipe, chosen because of its compatibility with kerosene, having $OD = 12$ mm and a larger $ID = 10$ mm, and hosts two titanium electrodes (purchased from SigmaAldrich, purity 99.98 %), each one having a width of 5 mm, length of 30 mm and thickness of 0.2 mm for a surface area in direct contact with the colloid equal to 300 mm^2. To create the hydraulic connection, two further pipes (having $OD = 7$mm and $OD = 10$mm) have been used, connecting them with some tube glass reinforced nylon 6.6 connectors (purchased by Legris, series LF 3000). To have a better comprehension of the apparatus, refer to **Figure 1** and its inset.

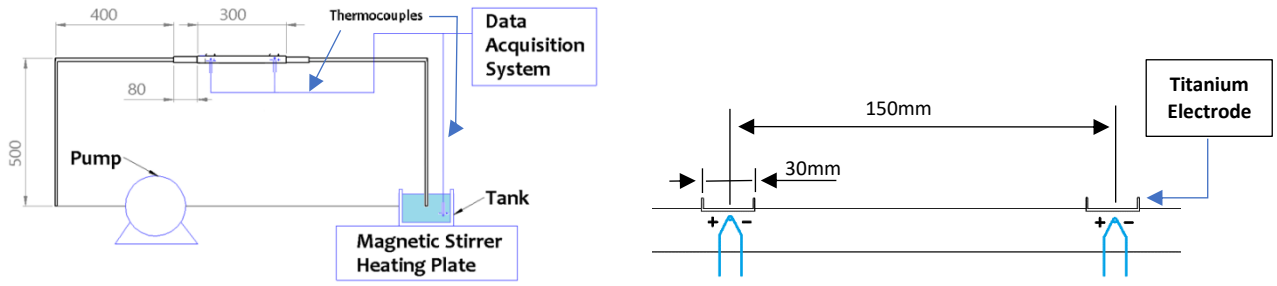


Figure 1: *Experimental apparatus for the characterization of the pyroelectric effect in a BT-based colloid: on the left overview of the complete system and on the right a focus of the central FEP pipe.*

The pump can generate a maximum flow rate of 100 $\frac{mL}{min}$ for each rotor coupled to the pipe. During these experiments only one rotor was used, to preserve a laminar flow in the fluid. Following the formula

$$Q = \langle v \rangle D^2 \frac{\pi}{4} \tag{1}$$

with Q indicating the volumetric flow rate, $\langle v \rangle$ [cm/s] the average fluid velocity and D the pipe diameter, we can change the actual average fluid velocity by varying the pump rotation velocity. In order to investigate different cooling rates, different volumetric flows have been set of 10, 20, 30, 50 and 100 $\frac{mL}{min}$ corresponding respectively to velocities of ≈ 0.2, 0.4, 0.6, 1.1, 2.2 $\frac{cm}{s}$ and Reynolds numbers ranging from about 10 to 100 guaranteeing a laminar flow regime in the entire velocity range. In fact, for the pure pyroelectric effect only, a turbulent flow is expected to give a positive contribution thanks to the vorticity allowing more BT nanoparticles to reach the electrode and release their charge per second but, because of their unstable nature, we preferred to avoid them. Considering that the overall mixture used, composed by kerosene and ferrofluid as carrier fluid and BT NPs in 0.5 %vol concentration, has a density $\rho = 922.6$ kg/m^3 and a dynamic viscosity $\mu = 2.13 \times 10^{-3}$ kg/(m·s), calculated using Einstein relation [20], we can express the Reynolds number as:

$$Re = \frac{\rho d v}{\mu} \tag{2}$$

where d [m] is the internal diameter of the FEP pipe and v [m/s] the mean fluid velocity.

Two heating conditions have been investigated: one named low-heating (LH), where the temperature increase in the reservoir was provoked only by mechanical stirring, and the other called strong-heating (SH), where the fluid in the reservoir was heated up to ≈ 60 °C before being pumped. Note that before each new flow velocity it was waited that the fluid would reach this temperature again. This is necessary since a reduction of about 10 °C in the becher's temperature occurred because of the cooling of the mixture during motion. The choice for this latter temperature is based on a trade-off among the solvent evaporation rate, the cooling rate and the time needed to heat up the solution. As shown in **Figure 1**, temperature was monitored in three notable points: the reservoir and in proximity of the two electrodes, by means of N- type thermocouples (Eltec Cables and Instruments). These have been calibrated and connected to a Data AcQuisition (DAQ) system (USB-6289 by National Instrument) controlled by means of LabView program for data manipulation.

In the sketch inset the extraction system installation can be noticed. The two electrodes are placed at a distance of 150 mm and sealed using high-strength two-component epoxy adhesive LOCTITE® EA 9455 (purchased from Henkel). Voltage and current versus time are acquired by means of two identical Keithley 2635A –SourceMeter® controlled remotely by LabView program for the data acquisition. These instruments are able to measure down to 1 pA currents and 1 nV potentials. To evaluate the energy conversion efficiency, different components of the colloidal suspensions have been analysed separately. In particular, kerosene, ferrofluid and the mixture KBT05 in both heating conditions have been forced separately in the system monitoring the temperature and acquiring current and voltage versus time meanwhile changing the pump rate.

3. Results

In order to verify the effective contribution to current and voltage given by BT, i.e. by PyE effect, the different components of the mixture have been investigated. Initially, the kerosene is pumped into the system at the different flow rates, corresponding to velocities of [0.21, 0.42, 0.63, 1.06, 2.12] $\frac{cm}{s}$, in both heating conditions. Neither PyE nor triboelectric behaviour is expected, neither voltage nor current was significantly measured above the noise floor. Kerosene plus 2 % vol FF mixture was also characterized in all the previous described conditions, and a remarkable triboelectrification of the fluid has been observed. Current and voltages are acquired to be subtracted from the colloid including 0.5 % vol BT NPs, in order to isolate the pure PyE component of energy generation. The maximum power extracted per unit area is given by Equation (1):

$$P_{PyE}^{Max}\big|_{A_s} = \frac{P_{PyE}}{l_{FEP}A_s} = \frac{V_5 \cdot I_5}{V_{eff}} \tag{3}$$

where V_5 and I_5 represent the voltage and current values at the fifth flow rate, namely $\langle v_5 \rangle = 2.12 \frac{cm}{s}$, V_{eff} is the effective volume obtained considering the pipe length l_{FEP} and its area A_s.

Data acquired by the thermocouples are reported in **Figure 2**: on the left the temperature acquired in typical LH condition is reported, i.e. with only stirrer providing thermal agitation, and on the right the temperature in typical SH condition, i.e. with hot plate bringing the colloid reservoir up to 60 °C. Standard deviation provided in the numbers as inset gives a measure of the excellent thermal stability of our measurements, where the gradient is marginal (lower than 0.096 ± 0.001 °C). When pumping is activated, at the highest temperature set, the colloid circulating back to the reservoir abruptly lowers the reservoir temperature. Approximately after 200 s a steady condition is achieved and the gradient between the two electrodes stabilizes at 2.354 ± 0.004 °C. Notice that with electrode 1 is indicated the first electrode encountered by the flowing mixture while the 2 indicates the farther.

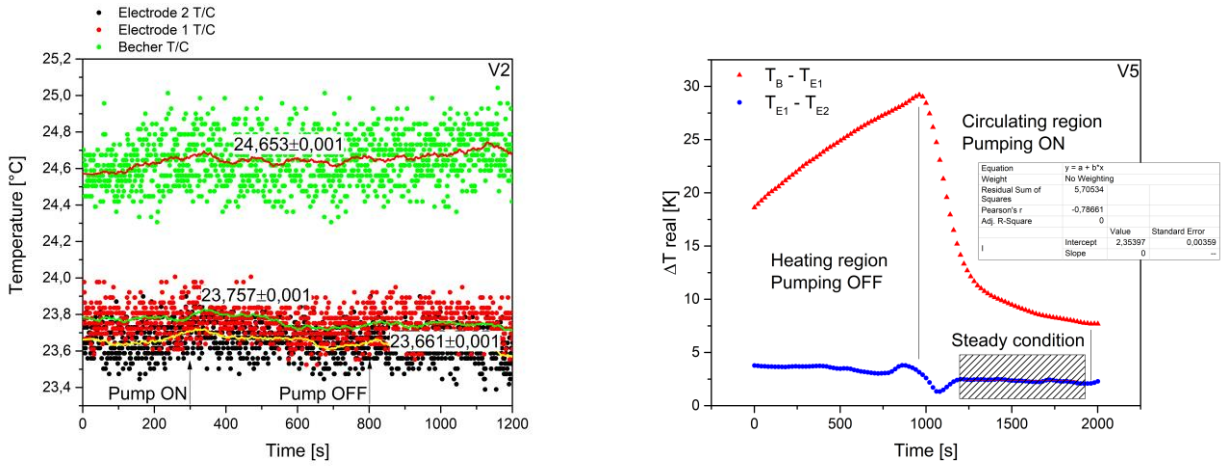


Figure 2: *Temperature trend in typical a) LH and b) SH condition. The smoothed curves are obtained using a first order Savitzky-Golay filter over a window including 59 experimental points. In panel b) only the gradients have been shown, calculated subtracting the smoothed curves.*

In order to provide the complete set of temperatures in both conditions, **Table 1** and **2** are reported, with the temperature of becher (B), first (E_1) and second (E_2) electrodes and the temperature difference ($\Delta T_{B,E1}$) in low and strong heating conditions, respectively.

Temperature	$\langle v \rangle_1$	$\langle v \rangle_2$	$\langle v \rangle_3$	$\langle v \rangle_4$	$\langle v \rangle_5$
Becher (T_B)	24.7 ± 0.1	24.8 ± 0.1	24.7 ± 0.1	24.8 ± 0.1	24.8 ± 0.1

Electrode 1 (T_{E_1})	23.9 ± 0.1	23.8 ± 0.1	23.8 ± 0.1	23.7 ± 0.1	23.8 ± 0.1
Electrode 2 (T_{E_2})	23.8 ± 0.1	23.5 ± 0.1	23.6 ± 0.1	23.5 ± 0.1	23.5 ± 0.1
$\Delta T_{B,E_1}$	0.8 ± 0.2	1.0 ± 0.2	0.9 ± 0.1	1.1 ± 0.2	1.0 ± 0.2

Table 1: *Set of temperatures acquired during the experiments in low heating condition.*

Temperature	$\langle v \rangle_1$	$\langle v \rangle_2$	$\langle v \rangle_3$	$\langle v \rangle_4$	$\langle v \rangle_5$
Becher (TB)	47.0 ± 0.1	50.6 ± 0.1	49.0 ± 0.3	50.1 ± 0.2	47.8 ± 0.1
Electrode 1 (T_{E_1})	27.2 ± 0.1	29.9 ± 0.1	34.3 ± 0.1	35.2 ± 0.1	29.7 ± 0.3
Electrode 2 (T_{E_2})	24.6 ± 0.1	26.7 ± 0.1	31.4 ± 0.1	32.1 ± 0.1	25.8 ± 0.2
$\Delta T_{B,E_1}$	19.8 ± 0.2	20.7 ± 0.2	14.7 ± 0.2	14.9 ± 0.2	18.1 ± 0.2

Table 2: *Set of temperatures acquired during the experiments in strong heating condition.*

Figure 3 reports the voltage and current versus time in LH conditions, to provide the reader an example of typical instrumental readings. The behaviour is quite stable, until 0.63 cm/s; after this speed, it is possible to see how both potential and current are slowly moving to an asymptote, increasing and decreasing, respectively. This might be due to charge extraction limitations in the system and to the different entrance length E_L between the different velocities. In fact, this latter identifies the space needed to completely develop the flow profile of the mixture in the pipe and can be computed according to the formula:

$$E_L = 0.06\, Re \cdot d \tag{4}$$

with d pipe inner diameter. Substituting the values for the lowest and highest flow rates, the entrance length passes from 5 mm to 5,5 cm, respectively. This led to a completely developed profile in proximity of the first electrode in the case of low flow rates but in a not completely developed one for rates higher than 50 mL/min.

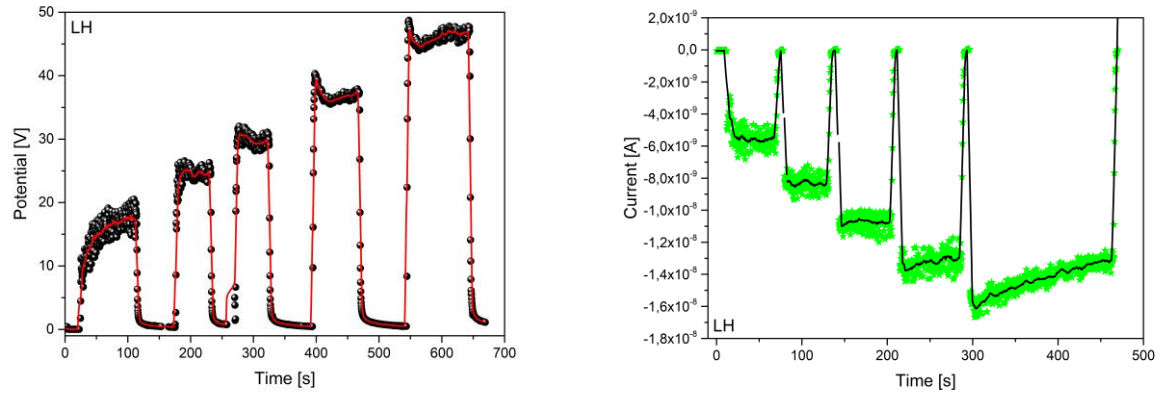


Figure 3: *Voltage versus time (a) and current versus time (b) acquired by means of a source meter during KBT05 motion at different flow rates low-heating conditions.*

All experimental readings have been fitted, subtracted by the solvent ones (given by kerosene plus stabilizing FF) and plotted in **Figure 4**, where each value of potential and current has been normalized by the FEP tube length to give electric fields and by the electrode area to give current densities. Interestingly, the sign of the current density changes by exploiting active heating and PyE effect, while the electric field does not change sign and slightly increases. The effect of velocity produces a steady but nonlinear increase in electric fields and also a nonlinear increase in the currents, where in LH conditions a peak is seen. There is a significant increase in power production, especially at intermediate velocities, in SH condition. This could be related to a decrease in viscosity [21, 22] which consequently leads to a lower friction among the NPs and the surrounding solvent, allowing a larger number of NPs to reach the electrodes.

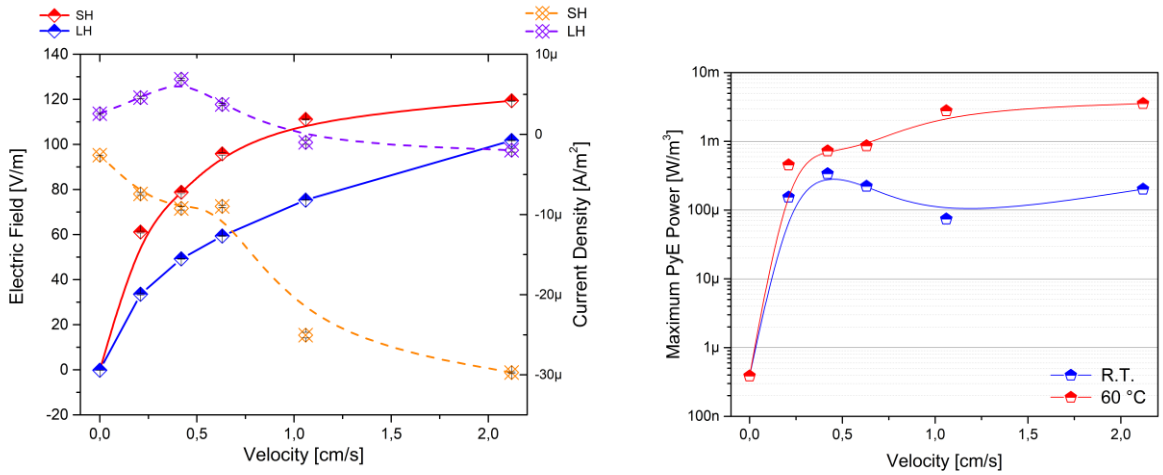


Figure 4: *Electric field and current density (a) as a function of the colloid velocity and heating condition. Maximum power (b) as a function of the colloid velocity and heating condition. Numbers have been given for the pure PyE effect, decoupling triboelectrification of solvent carrier and subtracting its contribution.*

4. Discussion

To better frame the PyE effect and understand how it is connected to the main physical quantities we can refer to the Heckmann diagram reported in **Figure 5**. [23]

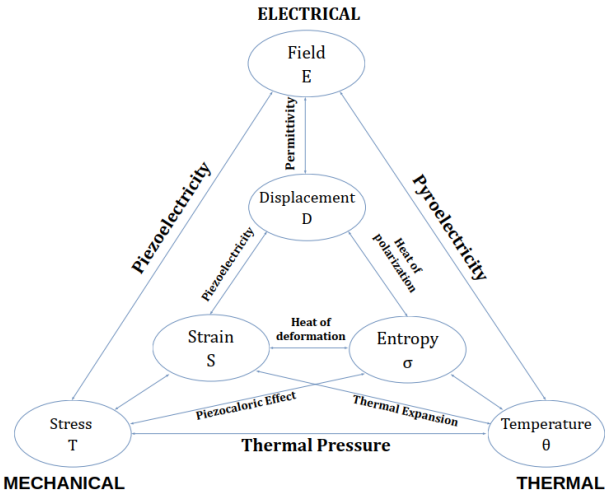


Figure 5: *Heckmann diagram*

This allows, using the works of Srinivasan [24] and Jachalke [25], to write the PyE coefficient p in a complete and exhaustive way, accounting all those phenomena contributing to the primary or secondary PyE coefficient:

$$p_l = \frac{\partial P_{S,l}}{\partial T} + \sum_{i,j} \frac{\partial d_{l,i,j}\sigma_{i,j}}{\partial T} + \sum_{i,j,k} \frac{\partial}{\partial T}\left(\mu_{l,i,j,k}\frac{\partial \pi_{i,j}}{\partial r_k}\right) + \sum_{l,i} E_i \frac{\partial \varepsilon_{l,i}}{\partial T} \tag{5}$$

where the subscripts i, j, k, l span on the Cartesian coordinates (x, y, z), P_S is the spontaneous polarization, T is the temperature, $\sigma_{i,j}$ is the mechanical stress, , $d_{i,j,k}$ is the piezo-electric coefficient, $\mu_{i,j,k,l}$ is the flexoelectric coefficient, $\pi_{i,j}$ represents the strain tensor, r_k indicates the position of the point of interest and E_i is the i-*th* component of the electric field with $\varepsilon_{l,i}$ coefficient of electric field induction.

In order to associate the increase in current and voltage outputs, observed in previous section, to the pyroelectric current, the pyroelectric coefficient must be evaluated. Because of the nature of the characterization and the structure of the system, the so-called *contact approach* method is suitable for its estimation [25]. This is a static approach, i.e. a method where the temperature gradient is maintained constant, in which it is possible to extract a compact formula only for the primary pyroelectric coefficient p_I. It does not allow the evaluation of the other components since there is neither uniform or

spatially varying viscous stress, needed to evaluate the secondary and tertiary components, nor electric field are applied. Thus, the charge developed on each BT NPs experiencing a temperature variation dT can be written as:

$$dQ_k = p_I \cdot A_k \cdot dT \tag{6}$$

with A_k representing the surface of the k-th particle. Assuming linear temperature decrease from the becher to the first electrode, accounting for the time employed by the particle to reach the latter and assuming that the charge is released entirely there, the overall charge on the electrode can be rewritten according to following expression: [26]

$$Q = \int_0^{\Delta T_{B,E_1}} N_c \cdot p_I \cdot A \cdot dT \tag{7}$$

Being interested in the volume of fluid in contact with the electrode, the attention is focused on a column of fluid V with height equal to the electrodes length l_e = 3 $\pm$ 0:1 cm and radius equal to r = 5mm. A indicates the contact area of the nanoparticles with the electrode that must be evaluated accounting for the spatial distribution of BT NPs and their deformation occurring during the contact. Considering homogeneous distribution and considering a small parallelepiped V_c having area A_e and thickness equal to the NPs diameter, the number of particles in contact with the electrode is:

$$N_c = \frac{V_c \cdot c}{V_{BT}} \tag{8}$$

with c indicating the barium titanate volume concentration. According to the work of Jachalke *et al.* [25] the pyroelectric coefficient can be expressed as:

$$p_I = \frac{I_p \cdot C_M}{A \cdot F_h} \tag{9}$$

where I_p represents the pyroelectric current, C_M the heat capacity of BT, A the effective electrodes area and F_h the heat flux. Since this latter is mainly due to forced convection, it can be defined using the Fourier's law in one dimension, assuming x to be the direction parallel to the electrodes area, as:

$$F_h = -\kappa \frac{dT(x)}{dx} \tag{10}$$

where the temperature spatial distribution is known and κ is the BT thermal conductivity. The only parameter which has not been yet analysed is the contact area A. In fact, the deformation of the particle hitting the electrode surface must be accounted. In the work of Greenwood and Williamson [27] it has been proven that, for deformations lower than 40 %, i.e. for rigid structures, the Jackson and Green [28] formula for elasto-plastic contact can be used:

$$\frac{a}{R} = \sqrt{\frac{\omega}{R}}\left(\frac{\omega}{1.9\omega_c}\right)^{\frac{B}{2}} \tag{11}$$

with a radius of the deformed region, $\omega_c = \left(\frac{\pi c S_y}{2E}\right)^2 R$ the critical indentation [29], $c = 1.295 \exp(0.736\nu)$ being ν the Poisson ratio. B is a material parameter that accounts the relation among the yield strength S_y and E the Young's modulus according to

$$B = 0.14 \exp\left[23 \cdot \frac{S_y}{E}\right] \tag{12}$$

According to some studies [30, 31] in which the barium titanate mechanical properties have been investigated as function of temperature, the Young's modulus vary from 116 GPa at $T = 340$K to 85 GPa at $T = 300$K, the yield strength is $S_y =$ 486.2 MPa and the Posson ratio is $\nu = 0.35$.

Substituting these values in the above expressions it was possible to estimate the effective electrode contact area in both heating conditions to be:

$$\begin{aligned} A_{LH} &= N_c \cdot \pi \cdot a_{LH}^2 = 147 \pm 1\ \mu m^2 \\ A_{SH} &= N_c \cdot \pi \cdot a_{SH}^2 = 79 \pm 1\ \mu m^2 \end{aligned} \tag{13}$$

In **Table 3** are summarized the pyroelectric coefficients in calculated for the medium high velocities in both heating conditions for BT05 mixture.

	$\langle v \rangle_3$	$\langle v \rangle_4$	$\langle v \rangle_5$
$p_{I,LH}, \left[\frac{\mu C}{m^2 K}\right]$	2.53	2.40	2.48
$p_{I,SH}, \left[\frac{\mu C}{m^2 K}\right]$	3.05	3.75	3.57

Table 3: *Pyroelectric coefficient calculated in both heating condition for KBT05 mixture*

The experimental values obtained are comparable with the one reported in literature for a temperature lying around T = 300K [32]. Thus, BT effectively enhances the performances of current production thanks to the PyE charge released on the electrode and the contribution observed during the measurements can be related to the PyE effect. Moreover, the increase in this figure of merit switching from LH to SH condition is coherent with the data reported in literature [32], varying from $\approx 2.2\ \mu C\ m^{-2}K^{-1}$ at 300K to $3.7\ \mu C\ m^{-2}K^{-1}$ at 340K.

As a final analysis, the conversion efficiency of the system is evaluated accounting for all the source of power in input and comparing with the electrical power extracted. To do so, the first contribution to be considered is provided by the stirrer that, because of mechanical agitation, provokes an increase in temperature $\Delta T_{stir} \approx 1.5$ °C with respect to the room temperature of 23°C, as can be appreciated in **Figure 2**a. According to the theory of mixing, the power transferred to the fluid during mechanical agitation depends on variables such as the size of the tank and impeller, fluid properties such as viscosity, and stirred speed. It has been determined experimentally for a variety of situation varying those parameters [33] and in particular the impeller shape, here represented by an anchor. The relationship between these variables is usually expressed in terms of dimensionless numbers, such as the impeller Reynolds number (Re) and the power number N_p. According to [33] the Reynolds number in of the stirred fluid can be expressed as

$$Re = \frac{N_i \, \rho_m \, D^2}{\mu_m} \tag{14}$$

with N_i representing the stirring speed (rps), D^2 the anchor length and μ_m the mixture kinematic viscosity. This fundamental parameter allow to determine the turbulent regime of the mixture inside the becher so that the power number $N_p = 0.35$. [33] Having this, the power transferred to the fluid during mixing can be expressed as:

$$P_{stir} = N_p \, \rho_m \, N_i^3 \, D^5 \tag{15}$$

Finally, the second contribution is given by the heating plate in strong heating conditions. To calculate the amount of heat transferred to the fluid it can be used the well-known heat formula

$$Q_h = \Delta T_h \cdot m_b \cdot C \tag{16}$$

where m_b represents the mass of the mixture contained in the becher and C its specific heat capacity that can be computed according to [34]

$$C = \frac{(1 - \varphi - \theta)\rho_f C_f + \varphi \rho_{FF} C_{FF} + \theta \rho_{BT} C_{BT}}{\rho_m} \tag{17}$$

where ρ_f is the carrier fluid density, φ and ρ_{FF} are the concentration and the density of magnetite, θ and ρ_{BT} are the concentration and the density of barium titanate, while C_f, C_{FF} and C_{BT} are the specific heat capacities of the mixture's components. The mixture density can be computed using [35]

$$\rho_m = (1 - \varphi - \theta)\rho_f + \varphi \rho_{FF} + \theta \rho_{BT} \tag{18}$$

Considering that the fluid, in SH condition, is always heated up to 60°C before each experimental flow rate, the temperature difference that must be considered is $\Delta T_h = 37$ °C, giving

$$P_h = \dot{Q}_h = \frac{\Delta T_h \cdot m_b \cdot C}{t_h} \tag{19}$$

with t_h time needed to reach the temperature of 60 °C. As a final step, the power provided by both stirrer and heater must be normalized on the becher's volume (V_b) considering the volume of fluid effectively drawn up (V_d). This must to be done in order to keep into account as useful power, just the amount provided to the liquid which is actually used to produce the electrical power output, avoiding to consider the one dispersed in the fluid remaining in the becher. Thus, the total input power P_I per unit volume, in order to be consistent with previous notation, will be given by the sum of all these contributions

$$P_I = \frac{\overline{P_{stir}} + \overline{P_h}}{V_{norm}} = \frac{1}{V_{norm} \cdot V_b}(P_{stir}V_d + P_h V_d) \tag{20}$$

with V_{norm} indicating the normalization volume obtained accounting the length of the FEP pipe and the electrodes area. To summarize, the results are shown in Table 5, where the evaluation of the overall efficiency η_{all} of the system, accounting all the contribution to the output power, and the pyroelectric efficiency η_{PyE}, obtained accounting the pure PyE effect decoupling triboelectrification of solvent carrier, in both heating conditions have been reported.

	$\langle v \rangle_1$	$\langle v \rangle_2$	$\langle v \rangle_3$	$\langle v \rangle_4$	$\langle v \rangle_5$
η_{all}^{LH}	1.47 %	1.57 %	1.61 %	1.52 %	1.15 %
η_{all}^{SH}	2.33 %	2.49 %	2.17 %	1.89 %	1.12 %
η_{PyE}^{LH}	0.28 %	0.31 %	0.14 %	0.03 %	0.04 %
η_{PyE}^{SH}	0.7 %	0.57 %	0.45 %	0.87 %	0.56 %

Table 4: *Efficiencies of the system with the KBT05 mixture flowing at different velocities, in both LH and SH conditions. The subscript all indicated the efficiencies obtained considering all the mixture components while PyE indicates those obtained considering the only pyroelectric effect.*

In conclusion we show the overall power extraction capability of the setup, including both the PyE from BT NPs and the triboelectric effect generated by the kerosene dispersion of FF, in **Figure 6**.

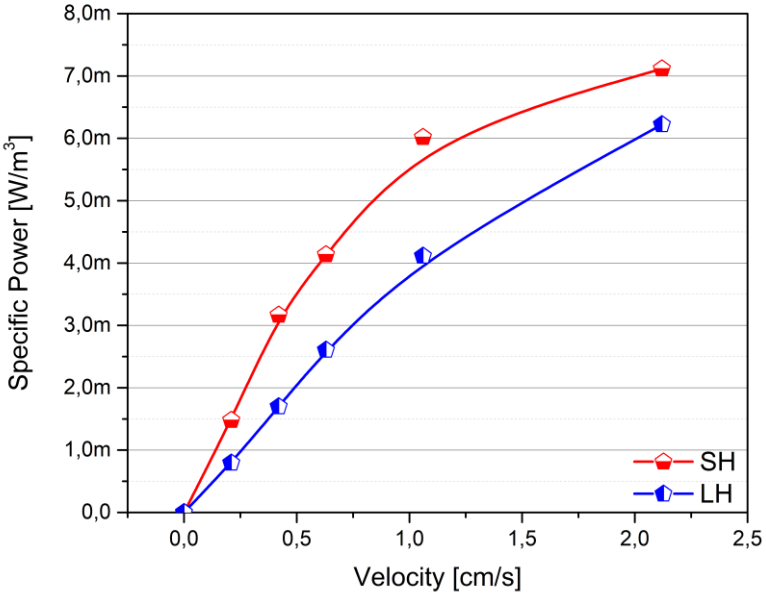


Figure 6: *Maximum power as a function of the colloid velocity and heating condition. Numbers have been given for the pure PyE effect, decoupling triboelectrification of solvent carrier and subtracting its contribution.*

5. Conclusions

In conclusion we have realized a one of a kind prototypes, based on a colloidal suspension of tetragonal barium titanate nanoparticles stabilized by a ferrofluid, for liquid state pyroelectric energy generation. Titanium electrodes have demonstrated to enable galvanic extraction, that allowed to directly measure the open circuit voltage and short circuit current. Triboelectrification of the colloid components has been subtracted to evaluate the proper pyroelectric effect, over small temperature gradients and velocity ranges comparable to those enabled by natural convection. A comprehensive theoretical corpus was introduced to evaluate the hydrodynamic properties of the flux, the pyroelectrification as a function of the temperature gradients and the charge transfer efficiency between pyroelectric nanoparticles and metallic electrodes. Our results show that the liquid state pyroelectric harvester represents a promising route to increase the sustainability and efficiency of industrial processes and place a milestone in the field of Waste Heat to Power technologies.

References

[1] International Energy Agency, “World Energy Outlook 2019,” EIA GOV, Washington, DC, 2019.

[2] British Petroleum Company, “BP Statistical Review of World Energy,” British Petroleum Co., London, 2019 | 68th edition.

[3] C. Forman, I. K. Muritala, R. Pardemann and B. Meyer, “Estimating the global waste heat potential,” *Renewable and Sustainable Energy Reviews,* vol. 57, pp. 1568-1579, 2016.

[4] C. Park, H. Lee, Y. Hwang and R. Radermacher, “Recent Advances in Vapor Compression Cycle Technologies,” *International Journal of Refrigeration,* vol. 60, pp. 118-134, 2015.

[5] M. B. Elsheniti, O. A. Elsamni, R. K. Al-dadah, S. Mahmoud, E. Elsayed and K. Saleh, "Adsorption Refrigeration Technologies," *Sustainable Air Conditioning Systems,* pp. 71-94, 2018.

[6] T. Yamamoto, T. Furuhata, N. Arai and K. Mori, “Design and testing of the Organic Rankine Cycle,” *Energy,* vol. 26, pp. 239-251, 2001.

[7] E. Garofalo, M. Bevione, L. Cecchini, F. Matiussi and A. Chilerio, “Waste Heat to Power: Technologies, Current Applications and Future Potential,” *Article in Submission.*

[8] T. Torfs, V. Leonov and C. V. Hoof, “Body-Heat Powered Autonomous Pulse Oximeter,” *IEEE SENSORS,* pp. 22-25, 2006.

[9] V. Leonov, “Simulation of maximum power in the wearable thermoelectric generator with a small thermop,” *Microsystem Technology,* vol. 17, pp. 495-504, 2011.

[10] V. Leonov, “Thermoelectric Energy Harvesting of Human Body Heat for Wearable Sensors,” *IEEE SENSORS,* vol. 13, no. 6, pp. 2284-2291, 2013.

[11] V. Leonov, T. Torfs, P. Fiorini and C. V. Hoof, “Thermoelectric Converters of Human Warmth for Self-Powered Wireless Sensor Nodes,” *IEEE SENSORS JOURNAL,* vol. 7, no. 5, pp. 650-657, 2007.

[12] H. Xue, Q. Yang, D. Wang, W. Luo, W. Wang, M. Lin, D. Liang and Q. Luo, “A wearable pyroelectric nanogenerator and self-powered breathing sensor,” *Nano Energy,* vol. 38, pp. 147-154, 2017.

[13] H. Ryu and S.-W. Kim, “Emerging Pyroelectric Nanogenerators to Convert Thermal Energy into Electrical Energy,” *Small,* no. 1903469, pp. 1-21, 2019.

[14] A. Chiolerio, E. Garofalo, L. Cecchini and M. Bevione, “Multieffect Liquid State Thermal Harvester (MU-STAR)”. Torino/Piemonte Patent In grant procedure.

[15] E. Garofalo and M. B. A. C. Luca Cecchini, “Triboelectric characterization of colloidal TiO2 for energy harvesting applications,” *MDPI,* vol. Article in submission, 2020.

[16] A. Chiolerio and M. B. Quadrelli, “Colloidal Energetic Systems,” *Energy Technology,* vol. 7, no. 5, pp. 1-30, 2019.

[17] A. Isse, "Crystal Hybridized Pyro-Piezoelectric Ferrofluidic Harvester".

[18] L. Jin, Y. Zhang, Y. Yu, Z. Chen, Y. Li, M. Cao, Y. Che and J. Yao, “Self-Powered Colloidal Wurtzite-Structure Quantum Dots Photodetectors Based On Photoinduced-Pyroelectric Effect,” *Advanced Optical Materials,* no. 1800639, pp. 1-8, 2018.

[19] I. A. Materials, “Barium Titanate (Barium Titanium Oxide, BaTiO3) powder,” Advanced Materials, [Online]. Available: http://www.advancedmaterials.us/5622-ON5.htm. [Accessed 23 07 2020].

[20] A. Hughes, "The Einstein Relation between Relative Viscosity and Volume Concentration of Suspensions of Spheres.," *Nature,* vol. 173, p. 1089–1090, 1954.

[21] J. N. Angaitkar and D. A.T.Shende, “Temperature dependent Dynamic (Absolute) scosity of Oil,” *International Journal of Engineering and Innovative Technology,* vol. 3, pp. 449 - 454, 2008.

[22] T. M. Harms, M. A. Jog and R. M. Manglik, “Effects of TemperatureDependent Viscosity Variations and Boundary Conditions on Fully Developed Laminar Forced Convection in a Semicircular Duct,” *Journal of Heat Transfer,* vol. 120, pp. 600-604, 1998.

[23] S. B. Lang, Sourcebook of pyroelectricity, London: Gordon and Breach Science Publishers , 1974.

[24] M. Srinivasan, “ Pyroelectric materials,” *Bulletin of Material Science,* vol. 6, no. 2, pp. 317-325, 1984.

[25] S. Jachalke, E. Mehner, H. Stöcker, J. Hanzig, M. Sonntag, T. Weigel, T. Leisegang and D. Meyer, “How to measure the pyroelectric coefficient,” *Applyed Physics Reviews,* vol. 4, no. 2, 2017.

[26] J. Xie, “Experimental And Numerical Investigation on Pyroelectric Energy Scavenging,” Virginia Commonwealth University, Virginia Commonwealth , 2007.

[27] H. Ghaednia and R. L. Jackson, “The effect of nanoparticles on the real area of contact, friction and wear,” *Journal of Tribology,* vol. 135, no. 4, pp. 1-10, 2013.

[28] S. S. Wadwalkar, R. L. Jackson and L. Kogut, “A study of the elastic-plastic deformation of heavily deformed spherical contacts,” *Journal of Engeneering Tribology,* vol. 224, no. 10, pp. 1091-1102, 2010.

[29] R. L. Jackson and I. Green, “A finite element study of elasto-plastic hemispherical contact against a rigid flat,” *Journal of Tribology,* vol. 127, no. 2, pp. 343-354, 2005.

[30] T. Trzepiecinski and M. Gromada, “Characterization of mechanical properties of barium titanate ceramics with different grain sizes,” *Material Science- Poland,* vol. 36, no. 1, pp. 151-156, 2018.

[31] B. L. Cheng, M. Gabbay, W. Duffy and G. Fantozzi, “Mechanical loss and Young's modulus associated with phase transitions in barium titanate based ceramics,” *Journal of Materials Science,* vol. 36, no. 1, pp. 4951-4955, 1996.

[32] B. Ertuğ, “The Overview of The Electrical Properties of Barium Titanate,” *American Journal of Engineering Research,* vol. 2, no. 08, pp. 1-7, 2013.

[33] R. R. HEMRAJANI and G. B. TATTERSON, “Mechanically Stirred Vessels,” in *Handbook of Industrial Mixing: Science and Practice*, John Wiley & Sons, Inc., 2003, pp. 345-390.

[34] J. Buongiorno, “Convective Transport in Nanofluids,” *Journal of Heat Transfer,* vol. 128, no. 1, pp. 240-250, 2006.

[35] N. S. Mousavi and S. Kumar, “Effective heat capacity of ferrofluids e Analytical approach,” *International Journal of Thermal Sciences,* vol. 84, no. 1, pp. 267-274, 2014.

[36] X. Zhang, M. He and Y. Zhang, “A review of research on the Kalina cycle,” *Renewable and Sustainable Energy Reviews,* vol. 16, p. 5309–5318, 2012.